DETERMINATION OF INTRINSIC PARAMETERS AND DEM PARAMETER CALIBRATION OF MULTI-COMPONENT PARTICLES IN MILLET THRESHING MIXTURES

/

谷子脱出物多组分颗粒本征参数测定与离散元参数标定

Zi-yang HUANG[1)], Dong-ming ZHANG*[1)], Shu-juan YI[1)], Jun-chao WAN[1)], Yi-fu CHEN[1)]
College of Engineering, Heilongjiang Bayi Agricultural University, Daqing/P. R. China
Tel: +86-459-13836826364; E-mail: zdm1105561622@163.com;
Corresponding author: Dong-ming Zhang

DOI: https://doi.org/10.35633/inmateh-78-53

Keywords: *millet threshing mixtures; seeds; millet panicle cluster; short stalk*

ABSTRACT

The millet threshing mixture is the primary material processed during post-combine cleaning operations and mainly comprises components such as seeds, millet panicle clusters, and short stalks. These components exhibit significant differences in material properties, which consequently affect cleaning efficiency. In this study, the morphological dimensions and mechanical parameters of each component in Longgu 31 millet threshing mixtures were systematically measured, including Poisson's ratio, elastic modulus, shear modulus, angle of repose, static and dynamic friction coefficients, and the coefficient of restitution. The discrete element method (DEM) was employed to establish particle models for millet seeds, millet panicle clusters, and short stalks. Key contact parameters—namely static and dynamic friction coefficients and the coefficient of restitution—were calibrated using the Plackett–Burman design, the steepest ascent method, and the Box–Behnken response surface methodology. The results reveal substantial differences in the physical parameters among the components. The calibrated simulation values of the angle of repose show high consistency with experimental results, with an average error of less than 5%, thereby validating the reliability of the model and parameter system. The robust model and key parameters obtained in this study provide a solid data foundation for elucidating the mechanism of material motion during millet cleaning and for optimizing the design of cleaning and screening equipment. The findings also provide valuable references for simulation studies on the cleaning of small-particle-size minor grains.

摘要

谷子脱出物是联合收获后清选环节的主要研究对象，主要包含籽粒、谷码、短茎秆等成分，这些成分的物料特性差异显著，进而影响清选效率。本研究针对龙谷 31 号谷子脱出物，系统测定了各组分颗粒的形态尺寸和力学参数，包括泊松比、弹性模量、剪切模量、堆积角、静/动摩擦系数和碰撞恢复系数等。采用离散元方法建立谷子籽粒、谷码和短茎秆颗粒模型，并结合 Plackett–Burman 设计、最陡爬坡法与 Box–Behnken 响应面法对关键接触参数（静/动摩擦系数和碰撞恢复系数）进行反演标定。结果表明，各组分的物理参数存在明显差异；标定后的仿真堆积角与物理试验结果高度一致（平均误差<5%），验证了模型及参数体系的可靠性。本研究所获得的关键参数和可靠模型为揭示谷子清选过程物料运动机理和清选筛分装置的优化设计提供了坚实的数据基础，对小粒径杂粮清选仿真研究具有重要参考价值。

INTRODUCTION

Millet is a significant minor grain crop in China and plays a central role in healthy diets (*Li et al., 2021; Sun et al., 2025; Chang et al., 2020*). However, due to their small size and the presence of a complex millet threshing mixture, the cleaning of millet seeds poses a significant challenge in combined harvesting operations (*Tao, 2025*). The millet threshing mixture is the direct target of the cleaning operation, primarily consisting of seeds, millet panicle clusters, and short stalks (*Liu et al., 2023*). Significant differences in physical properties such as particle size and shape exist among these components, directly influencing material movement patterns on the screen surface and screening efficiency (*Wensrich et al, 2012*). Therefore, precise modeling and parameter calibration of millet threshing mixture reveal two things (*Shu et al., 2022*).

First, they reveal the intrinsic mechanisms of material contact, bouncing, and stratification during cleaning. Second, they establish a robust theoretical foundation and provide critical data support for exploring millet cleaning and screening principles and optimizing cleaning equipment design (*Li et al., 2025*).

The discrete element method (DEM) is a numerical simulation and analysis tool that is widely employed to study the mechanical behavior of granular systems (*Chen et al., 2025; Shi et al., 2026*). The method involves discretizing continuous media into numerous independent particle units, thereby enabling the accurate reproduction of the complex physical processes occurring in bulk granular materials (*Li et al., 2025; Gao et al., 2024*). This is achieved by solving particle motion equations and contact mechanics models. The DEM has garnered significant attention and has found extensive application in the domain of agricultural processes (*Xun et al., 2025*). At present, a considerable number of experts worldwide employ discrete element simulation software to conduct theoretical research on parameter calibration in agricultural engineering (*Ao et al., 2023*). *Li H.,* (*2025*) utilized the discrete element method to calibrate parameters for wheat with varying moisture contents. Through Plackett-Burman tests and steepest ascent tests, they identified key parameters and established a stacking angle-discrete element parameter model using Box-Behnken tests. This provides convenient and reliable technical support for optimizing emergency rapid dehumidification processes for high-moisture wheat particles. *Liu Z.,* (*2025*), conducted DEM simulations on walnut kernels, thereby illustrating the generalizability of kernel contact parameters in the context of "material-machine" interactions. *Xie et al.,* (*2023*), employed the DEM method to simulate two varieties of white rice, offering crucial parameters and analytical underpinnings for the development of rice processing DEM models. *Sun et al.,* (*2024*), calibrated the parameters between soil particles and boundaries, employing a discrete element model-multiscale boundary element coupling (DEM-MBD) to analyze how soil coverage and compaction processes at different advance speeds affect seed placement. This study provides a theoretical foundation for optimizing soil coverage structures and compaction processes. *Awuah et al.,* (*2023*), studied S-shaped and fork-shaped shovels, establishing a DEM soil-crop model to assess the reliability of other root and tuber harvesting tools. *Xu et al.,* (*2021*), employed an automatic filling method to develop a non-spherical buckwheat seed model and conducted simulation and physical stacking tests using a bottomless cone lift method. This provided seed models and simulation contact parameters for mechanical development in buckwheat sowing, threshing, and hulling. A review of the existing literature reveals that the majority of studies have focused on conventional agricultural materials, with a paucity of research on non-spherical modeling and dynamic validation for small-seeded grains such as millet threshing mixtures. Consequently, the development of high-precision models and the implementation of systematic parameter calibration are imperative for enhancing the accuracy of cleaning simulations and elucidating separation mechanisms.

The objective of this study was to systematically determine the intrinsic parameters of millet threshing mixtures. To accomplish this, Longgu 31 threshing mixtures were used as the research subject, and the parameters were modeled and calibrated for seeds, millet panicle clusters, and short stalks, respectively. Discrete element models were constructed for seeds, millet panicle clusters, and short stalks. An efficient system for calibrating contact parameters was established through the implementation of Plackett-Burman experiments, steepest ascent experiments, and Box–Behnken response surface methods. The precise quantification of key parameters provides core data support for elucidating the intrinsic mechanisms of millet cleaning and innovating cleaning device designs.

MATERIALS AND METHODS

The Testing of Materials and Determination of Their Physical Parameters

Millet threshing mixture is a heterogeneous material generated during the threshing and separation stage of millet harvesting. This mixture primarily consists of millet seeds, husks, short stalks, and minute impurities. The formation of the subject is dependent upon mechanical actions such as rubbing, crushing, and impact from the threshing and separation device. These mechanical threshing actions break the anchoring structural bonds between grains and millet panicle clusters, as well as between millet panicle clusters and the parent ears, resulting in the detachment of grains from their maternal structures. This process is accompanied by the shedding of non-target components, ultimately forming a cohesive, poorly flowing mixture. The present study employs Longgu 31 millet as the subject of inquiry, opting for pivotal elements derived from the millet threshing mixture—namely seeds, millet panicle clusters, and short stalks—as the materials for experimentation. The millet threshing mixture and its constituent parts are illustrated in Figure 1.

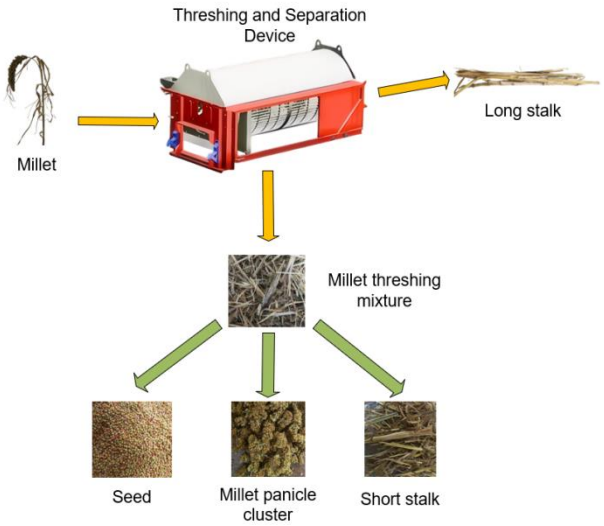

Fig. 1 - Millet threshing mixture and its constituents

Shape and Geometric Dimensions

Millet seeds exhibit a subglobular morphology, characterized by small size and low intrinsic weight. To systematically characterize the morphological attributes of these seeds, a sample set comprising 100 individual seeds was used. A high-precision electronic vernier caliper, with a resolution of 0.01 mm, was employed to obtain accurate dimensional measurements along the three principal axes of each seed.

Millet panicle clusters are irregular composite structures that form during the threshing of millet when seeds remain partially attached to small stalks. Due to the random nature of their formation, millet panicle clusters exhibit irregular shapes and sizes. To systematically characterize their dimensions and morphology, uniform samples were collected beneath the threshing drum, and representative specimens covering the primary grain size range were selected for analysis. A meticulous morphological examination revealed that millet panicle clusters could be categorized into four distinct structural types: spheroid, rectangular prism, pyramid-like, and ellipsoid, as illustrated in Figure 2. A sample of 100 representative specimens was selected from each category, and their geometric dimensions—length, width, and height—were precisely measured.

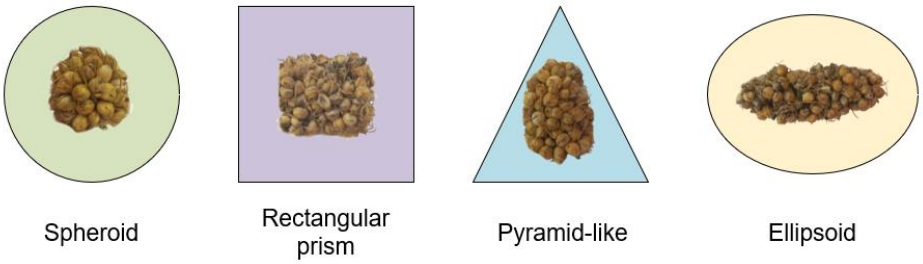

Fig. 2 - Structure of the millet panicle cluster morphology

Short stalks are fragments formed from broken stalks during the threshing process. They exhibit an overall slender morphology that can be approximated as short cylinders. Ten sampling positions were randomly selected along the axial direction of the threshing drum, and 30 stalk samples were collected at each position. Geometric parameters such as length and cross-sectional diameter were subsequently measured.

Investigation of the Millet Threshing Mixture and the Poisson's Ratio of Its Components

The Poisson's ratio is a term that refers to the ratio of the absolute value of transverse strain to axial strain when a material undergoes uniaxial tension or compression (*Xu et al., 2023*). This is also referred to as the transverse deformation coefficient. This parameter characterizes the coupled relationship between transverse and axial deformation in materials, and it serves as one of the core indicators describing the elastic deformation behavior of materials. The objective of this study was to ascertain the Poisson's ratio for a variety of representative samples, thereby refining the mechanical parameter modeling of millet threshing mixture particles. To accomplish this, an electronic universal testing machine was utilized, as illustrated in Figure 5(a).

The Poisson's ratio was determined through the use of an electronic universal testing machine, which enabled the execution of uniaxial compression tests on seeds, millet panicle clusters, and short stalks at a compression rate of 5 mm/min. Prior to testing, the initial sample dimensions were measured. Specimens were subjected to compression until achieving target deformations (0.8 mm for seeds, 3.2 mm for millet panicle clusters, and 2.5 mm for stalks) at a predetermined displacement rate. The dimensions before and after deformation were recorded, substituted into Eq. (1), and used to calculate Poisson's ratio.

$$v = \left|\frac{\varepsilon_1}{\varepsilon_2}\right| = \left|\frac{(A_1 - A_2)/A_1}{(B_1 - B_2)/B_1}\right| \quad (1)$$

where v is Poisson's ratio; ε_1 is strain of the transverse diameter of the material, mm; ε_2 is strain of the axial length of the material, mm; B_1 is length of the material before compression, mm; B_2 is length of the material after compression, mm; A_1 is diameter of the material before compression, mm; A_2 is diameter of the material after compression, mm.

Elastic Modulus and Shear Modulus of Each Component in Millet Threshing Mixture

The elastic modulus is defined as the ratio of stress to strain during a material's elastic phase, thereby characterizing its resistance to elastic deformation (*Shen et al., 2026*). This fundamental parameter serves as a core element in the domain of elastic mechanics. The shear modulus is also a key parameter in elastic mechanics, defined as the ratio of shear stress to shear strain. It characterizes a material's resistance to shear deformation. Similarly, an electronic universal testing machine was utilized to conduct uniaxial compression tests on seeds, millet panicle clusters, and short stalks at a compression speed of 5 mm/min. By analyzing the load and deformation in the elastic stage, the results were substituted into Eqs. (2) and (3) to calculate the elastic modulus and shear modulus of each component.

$$E_1 = \frac{(F_1 / A_3)}{\varepsilon} \quad (2)$$

$$G = \frac{E_1}{2(1+v)} \quad (3)$$

where E_1 is elastic modulus, MPa; F_1 is axial load borne by the material, N; A_3 is contact area, mm²;ε is strain; G is the shear modulus, MPa.

Angle of Repose for Various Components of Millet Threshing Mixture

The angle of repose is defined as the angle formed between the inclined surface of a naturally accumulated pile of granular material and the horizontal plane *(Yang et al., 2016)*. It serves as a macroscopic parameter characterizing the internal friction properties and flow behavior of the material. A measuring cylinder and a 45 steel plate were used as the main experimental apparatus to measure the angle of repose of seeds, millet panicle clusters, and short stalks, as illustrated in Fig. 3. The dimensions of the seed and millet panicle cluster samples were controlled within specified tolerance limits. During the test, the material was allowed to accumulate naturally into a conical pile within the chute. The angle measured between the generatrix of the pile and the horizontal plane represents the angle of repose of the material.

Fig. 3 - Natural accumulation of millet threshing mixture

Friction Coefficients of Different Parts of the Millet Threshing Mixture

The static friction coefficient represents the ratio of the frictional force to the normal force between two contacting surfaces. It characterizes the frictional interaction between materials. To evaluate the frictional behavior between particles in the millet threshing mixture and equipment surfaces, static and kinetic friction angle tests were conducted. The test apparatus consisted of a custom-built inclined plane tester, as shown in Fig. 5(b). A digital angle gauge with a resolution of 0.01° was used to measure the inclination angle. During the testing process, observations and measurements were carefully recorded to ensure the accuracy of the results.

The static friction coefficient is a dimensionless parameter that characterizes the resistance of two contacting objects to initial relative sliding when at rest. It is defined as the ratio of the maximum static friction force to the corresponding normal load. The static friction coefficient is determined by slowly raising the steel plate until the material reaches its critical slip point, as shown in Figure 4(a). The test procedure is outlined below. The inclined plane apparatus should be placed on a level reference platform, and the steel plate should be adjusted to its initial horizontal position. The material sample to be tested should be selected and then placed flat, contact surface down, on the steel plate. An external force should be applied to one end of the steel plate via the traction device, lifting the plate at a constant and slow speed so as to progressively increase the inclination acting on the sample. Lifting should be ceased immediately when the sample reaches critical slip. The angle α_1 between the steel plate and the horizontal plane should be recorded using an angle measurement device. The static friction coefficient is calculated using Eq. (4).

$$f_1 = \tan\alpha_1 \tag{4}$$

where f_1 is static friction coefficient; α_1 is critical angle of static friction, (°).

Employing the aforementioned method, the static friction coefficients between disparate materials were measured. Taking the static friction coefficient between seeds as an example, a uniform layer of seeds was fixed on the steel plate surface. Individual seeds were then placed on top for testing to obtain the static friction parameters between seeds. Similar methods were applied to measure static friction between other components, as demonstrated in Figure 5(b). A thorough statistical analysis of the experimental results was conducted, yielding invaluable insights into the static friction coefficients between millet threshing mixtures and the steel plate, as well as between different components of the millet threshing mixtures under a wide array of interaction conditions.

The rolling friction coefficient is a number that describes how much resistance there is at the point where two surfaces are in contact when they are rolling against each other. It is calculated by dividing the rolling friction torque by the normal pressure at the point of contact. The equipment and methods used in this study to measure the rolling friction coefficients of different parts of millet threshing mixture were the same as those used for measuring the static friction coefficients. For measurements, seeds with high sphericity and millet panicle clusters with excellent circular cross-sectional shape were selected. For placement, seeds were put with their wide, rounded backs against the base surface. Millet panicle cluster weights were put with their roundest parts touching the base. Stalk samples were arranged perpendicular to the direction of pulling. By gradually increasing the inclination angle, the material reached the point at which it began to roll down the inclined plane, as shown in Fig. 4(b). The angle α_2 between the inclined plane and the horizontal plane was then recorded. The rolling friction coefficient was calculated using Eq. (5).

$$f_2 = r\tan\alpha_2 \tag{5}$$

where f_2 is rolling friction coefficient; r is radius of gyration of the sphere, mm; α_2 is critical angle of rolling, (°).

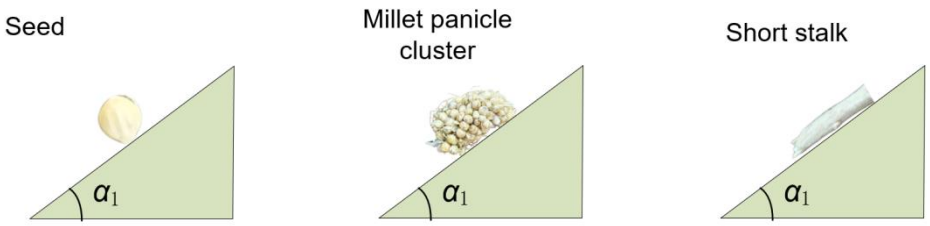

(a) Critical sliding state of material

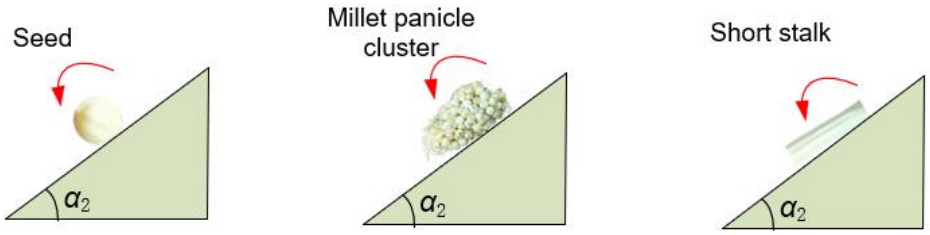

(b) Critical rolling state of material

Fig. 4 - State Diagram of Material Friction Coefficient

Coefficient of restitution

The coefficient of restitution is a dimensionless parameter that characterizes the degree of kinetic energy loss during collisions (*Wang et al., 2020*). Its value is equivalent to the ratio of the separation velocity of the two objects post-collision to their approach velocity pre-collision. The objective of this study was to measure the coefficient of restitutions between particles and between particles and walls. The wall material selected was 45 steel, which directly contacts the extracted material in the vibrating screen. The particle-particle coefficient of restitution was determined using a self-made air-blow collision testing apparatus, as illustrated in Figure 5(c).

During the testing phase, it is essential to initially level both glass tracks. The air pump should be activated and the pressure regulator utilized to adjust the airflow in both supply lines, thereby ensuring uniformity. Subsequent to deactivating the air pump, the material sample should be placed at the initial end of the glass track. The high-speed camera should then be activated, and the field of view and focus adjusted until a clear image is obtained, at which point recording should commence. The pump should be restarted and immediately shut off. The instantaneous driving force of the airflow should be used to propel the material along the track in a horizontal projectile motion, while simultaneously capturing video data of the collision process. The extracted data were substituted into Eq. (6) to calculate the coefficients of restitution between different materials.

$$e = \frac{V_{p1} - V_{p2}}{V_{p3} - V_{p4}} \tag{6}$$

where:

e is coefficient of restitution of collision between materials;

V_{p1} is the velocity of material 1 after collision, m/s;

V_{p2} is the velocity of material 2 after collision, m/s;

V_{p3} is the velocity of material 1 before collision, m/s;

V_{p4} is the velocity of material 2 before collision, m/s.

The particle-wall coefficient of restitution testing apparatus is a bespoke free-fall collision measurement device, as illustrated in Figure 5(d). During the experimental process, the steel plate is first positioned horizontally, with a vertical filming backdrop situated behind it to clearly capture the material's trajectory. The high-speed camera and LED lighting system are then activated, and the filming angle, focal length, and illumination parameters are adjusted to achieve optimal imaging conditions. The material sample is released to fall under the influence of gravity, thereby striking the steel plate surface. The resulting displacement and height data are recorded simultaneously during the falling and rebound phases.

The collected data were substituted into Eq. (7) to determine the coefficient of restitution between the material and the steel plate.

$$e = \sqrt{\frac{h}{H}} \tag{7}$$

where:

H is height of material falling, mm; h is height of material rebound, mm.11

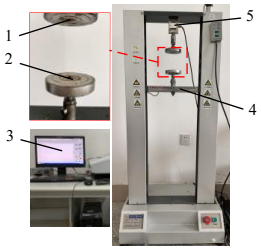

(a) Micro-control electronic universal material testing machine
1.Upper press head; 2.Lower conical section; 3.Data acquisition system; 4.Movable beam; 5.Force sensor

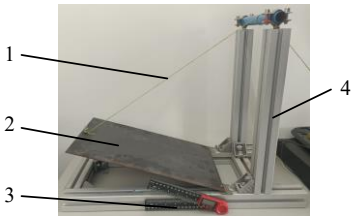

(b) Homemade Inclinometer
1.Leash; 2. 45 steel plate; 3. Digital angle gauge; 4. Mounting bracket

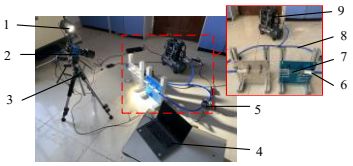

(c)Air-blown coefficient of restitution measuring device
1.Lighting lamp; 2. High-speed camera; 3. Mounting bracket; 4.Imaging system; 5.Pressure regulator; 6.Feed inlet; 7.Glass track; 8.Gas delivery tube; 9. Air compressor

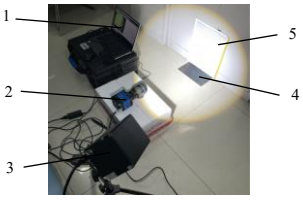

(d)Free-fall coefficient of restitution measuring device
1. Imaging system; 2. High-speed camera; 3. Lighting lamp; 4. Steel plate; 5. Background scale plat

Fig. 5 - Figure of Key Experimental Equipment

A Discrete Element Modeling Approach to the Analysis of Millet Threshing Mixture

The Discrete Element Method (DEM) provides the core theoretical and numerical framework for discrete element modeling of granular agricultural materials. It discretizes the research object into independent particle units and constructs mechanical interaction models between particles and between particles and boundaries. This enables numerical simulation of the motion and interaction processes within a discrete particle system. Discrete Element Modeling (DEM) provides an accurate numerical simulation platform for calibrating parameters of the millet threshing mixture. By establishing mechanical interaction models between particles and between particles and surfaces, DEM enables the inverse calibration of key parameters, such as friction coefficients and coefficient of restitutions. This approach significantly reduces the frequency and cost of physical experiments while enhancing parameter matching accuracy and reliability. Consequently, DEM offers scientific data support for structural optimization of threshing and cleaning equipment. In the present study, EDEM software was employed to model millet seeds, millet panicle clusters, and short stalks within the millet threshing mixture. Different filling methods were applied based on the test materials: manual filling was used for particles with high shape regularity, and automatic filling was used for particles with complex and variable shapes.

A Method for Calibrating the Parameters of Millet Threshing Mixture

In the context of discrete element simulation, the appropriate configuration of particle contact parameters emerges as a pivotal element influencing both the simulation accuracy and the physical consistency of the model. Consequently, subsequent to the completion of the geometric modeling of particles for each constituent of the millet threshing mixture, a meticulous calibration of their contact parameters becomes imperative. This calibration aims to bolster the precision and dependability of the simulation outcomes. The present study employs a Plackett–Burman experimental design to screen the key parameters that exert an influence on the target response value. The steepest ascent method is then utilized to rapidly approximate the optimal response region for the parameters. Finally, the Box–Behnken response surface optimization method is applied in order to obtain the optimal parameter combination that meets the experimental requirements. The calibration includes the static friction coefficient between particles, the rolling friction coefficient between particles and steel plates, and the coefficient of restitution.

RESULTS AND DISCUSSIONS

Shape and geometric dimensions

Using the aforementioned measurement method, 100 replicate measurements were conducted on the three-dimensional geometric dimensions of millet seeds, different morphological millet panicle clusters, and short stalks. The results showed that the mean values for millet seed length, width, and height were 1.55 mm, 1.51 mm, and 1.48 mm, respectively.

The corresponding standard deviations were 0.014, 0.009, and 0.007, while the standard errors were 0.0014, 0.0009, and 0.0007. Statistical analysis of size distribution indicated that all seed dimensions followed a unimodal, approximately normal distribution. The three-dimensional dimensions showed minimal variation, and the overall morphology was approximately spherical. Measurements were taken for four morphological categories: near-spherical, near-rectangular, near-conical, and near-ellipsoid. The dimensional ranges for each category were: maximum values of 11.13 mm, 11.27 mm, 10.76 mm, and 12.91 mm, respectively; minimum width values of 3.61 mm, 3.11 mm, 3.17 mm, and 3.78 mm, maximum width values of 10.87 mm, 10.99 mm, 11.51 mm, and 9.61 mm, respectively. The minimum values in the height direction were 3.65 mm, 3.48 mm, 4.95 mm, and 3.61 mm, respectively, while the maximum values were 11.29 mm, 10.82 mm, 12.37 mm, and 10.27 mm, respectively. The minimum length of the short stalk was 7.11 mm, with a maximum length of 128.77 mm. The minimum cross-sectional diameter of the short stalk was 1.53 mm, and the maximum cross-sectional diameter was 5.78 mm.

Poisson's ratio

The present study experimentally investigated the Poisson's ratio of millet seeds, millet panicle clusters, and short stalks. A total of 10 Poisson's ratio determination tests were conducted on these materials. The mean value of each group was taken as the final test result, yielding Poisson's ratios of 0.38, 0.37, and 0.26, respectively. The Poisson's ratio test results for each component of the millet threshing mixture are presented in Table 1.

Table 1

Poisson's ratio of each component in the millet threshing mixture

Number	Poisson's ratio of seeds	Poisson's ratio of millet clusters	Poisson's ratio of short stalks
1	0.37	0.36	0.25
2	0.38	0.37	0.26
3	0.39	0.38	0.27
4	0.37	0.36	0.25
5	0.38	0.37	0.26
6	0.39	0.38	0.27
7	0.38	0.37	0.26
8	0.37	0.36	0.25
9	0.39	0.38	0.27
10	0.38	0.37	0.26
Mean	0.38	0.37	0.26
Standard deviation (SD)	0.0082	0.0082	0.0082
Standard error (SE)	0.0026	0.0026	0.0026

Elastic modulus and shear modulus

The present study encompassed a total of 10 tests, with each test focusing on the elastic modulus and shear modulus of millet seeds, millet panicle clusters, and short stalks from millet threshing mixtures. Through meticulous analysis, the elastic modulus and shear modulus of each component were successfully calculated, culminating in the following set of results: the average elastic modulus of the millet panicle cluster was determined to be 0.43 MPa, with an average shear modulus of 0.16 MPa. Similarly, the average elastic modulus of the short stalks was found to be 3.61 MPa, with an average shear modulus of 1.45 MPa.

Angle of repose

In accordance with the aforementioned methodology, a series of ten angle of repose tests was conducted, with each test conducted on a separate sample of millet seeds, millet panicle clusters, and short stalks from the millet threshing mixture. The millet seeds, the conical pile formed by the natural fall of short stalks from a graduated cylinder was measured to determine the angle of repose. An angle gauge was utilized to measure the angle between the outer edge of the pile and the horizontal plane. The analysis yielded the following average angles of repose: 27.34° for millet seeds, 30.93° for millet panicle cluster, and 24.17° for short stalks.

Friction coefficient

A series of friction coefficient tests were conducted on an assortment of components derived from the millet threshing mixture. Through the comprehensive analysis of test data from each group, the static and rolling friction coefficients between the mixture and steel plates, as well as between various mixture components, were systematically summarized. The specific results of these analyses are presented in Tables 2 and 3, respectively.

Table 2

Static friction coefficient measurement results

Material - Material	Static friction coefficient	Material - Steel plate	Static friction coefficient
Seed - Seed	0.48 - 0.72	Seed - Steel plate	0.40 - 0.68
Seed - Millet panicle cluster	0.60 - 0.82	Millet panicle cluster - Steel plate	0.46 - 0.79
Seed - Short stalk	0.51 - 0.75	Short stalk - Steel plate	0.37 - 0.73
Millet panicle cluster - Short stalk	0.52 - 0.86		
Millet panicle cluster - Millet panicle cluster	0.60 - 0.77		
Short stalk - Short stalk	0.52 - 0.78		

Table 3

Rolling friction coefficient measurement results

Material - Material	Rolling friction coefficient	Material - Steel plate	Rolling friction coefficient
Seed - Seed	0.01 - 0.07	Seed - Steel plate	0.01- 0.05
Seed - Millet panicle cluster	0.01 - 0.07	Millet panicle cluster - Steel plate	0.02 - 0.09
Seed - Short stalk	0.02 - 0.09	Short stalk - Steel plate	0.01 - 0.04
Millet panicle cluster - Short stalk	0.02 - 0.08		
Millet panicle cluster - Millet panicle cluster	0.01 - 0.09		
Short stalk - Short stalk	0.01 - 0.07		

Coefficient of restitution

A series of self-blow collision tests were conducted on an array of components pertaining to the millet threshing mixture. Statistical analysis of the test data yielded the coefficients of restitution for the following contact pairs: seed–seed, seed–millet panicle cluster, seed–short stalk, millet panicle cluster–millet panicle cluster, millet panicle cluster–short stalk, short stalk–short stalk. The results are presented in Table 4.

Table 4

Measured coefficients of restitution for inter-particle collisions in the millet threshing mixture

Contact pair	Coefficient of restitution	Contact pair	Coefficient of restitution
Seed - seed	0.38 - 0.42	Seed - short stalk	0.28 - 0.40
Seed - millet panicle cluster	0.24 - 0.33	Millet panicle cluster - millet panicle cluster	0.26 - 0.31
Millet panicle cluster - short stalk	0.24 - 0.39	Short stalk - short stalk	0.30 - 0.45

In order to ascertain the coefficient of restitution between the millet threshing mixture and the wall surface, free-style coefficient of restitution measurements were conducted for seeds against 45 steel plates, millet panicle clusters against 45 steel plates, and short stalks against 45 steel plates. A subsequent statistical analysis of the coefficient of restitutions between particles and the wall surface yielded the specific results shown in Table 5.

Table 5

Measured coefficients of restitution between millet threshing mixture particles and steel plates

Contact pair	Coefficient of restitution
Seed - steel plate	0.38 - 0.48
Millet panicle cluster - steel plate	0.26 - 0.38
Short stalk - steel plate	0.32 - 0.46

Discrete Element Modeling

Millet Seed Modeling

Among the millet threshing mixture, seeds constitute the largest proportion by mass and quantity, serving as the primary component of the particle system. While the actual appearance of seeds is not perfectly spherical, they exhibit a more spherical shape compared to millet panicle clusters and short stalks. Based on statistical measurements of 100 millet seeds, their average length, width, and thickness were 1.55 mm, 1.51 mm, and 1.48 mm, respectively. These three-dimensional dimensions are highly consistent with minimal variation, indicating a full and uniform shape. Morphologically, they are near-spherical particles with negligible deviation from a spherical model, and the geometric error introduced by simplification remains within acceptable limits. Furthermore, the spherical model offers advantages in discrete element simulation, including computational stability, high efficiency, and a well-established parameter system. It also aligns with general specifications for grain material simulation. Therefore, this study simplifies millet seeds into spherical particles for modeling. Based on prior measurement data, the radius of the spherical model is set to 0.75 mm, as illustrated in Figure 4(a).

Millet Panicle Cluster Modeling

Millet panicle clusters exhibit high morphological complexity and structural diversity, classifying them as irregular particles. Existing studies often simplify millet panicle clusters into uniform regular particles, modeling them with standardized particle sizes and average parameters, thereby neglecting their true irregular shapes and wide size ranges. The actual morphology of millet panicle clusters is a loose, porous irregular structure, fundamentally differing from the contact and friction characteristics of regular rigid bodies. Differences in intrinsic properties such as grain type, moisture content, and degree of fragmentation directly alter the material's mechanical and surface characteristics. Prior to modeling, based on morphological studies of millet panicle clusters, structural statistical analysis of a large sample set classified millet panicle clusters into four categories: spheres, cuboids, cones, and ellipsoids. The length distribution of millet panicle clusters of different shapes is shown in Figure 6(a), the width distribution in Figure 6(b), and the height distribution in Figure 6(c). After experimental analysis, given the wide particle size range of millet panicle clusters (3 mm ≤ Rgm ≤ 13 mm), the 8 mm particle size sample, which has a high statistical proportion, was selected as the representative sample in this study. Boundary contour dimensions for each shape were determined, and a basic geometric model was established accordingly. For millet panicle clusters with Rgm ≠ 8 mm, geometric dimensions were adjusted using proportional scaling. This approach enabled shape representation of clusters of varying sizes within a unified modeling framework. The refined modeling in this study more accurately reflects the movement differences between millet panicle clusters and seeds, enhancing the reliability of cleaning and separation process simulations. This provides a robust foundation for optimizing cleaning equipment design.

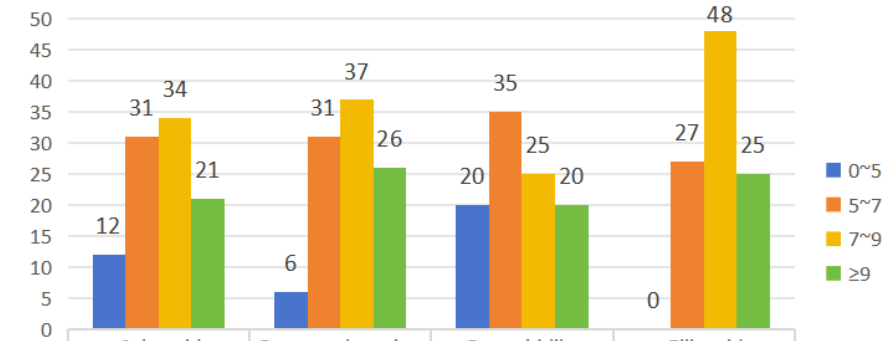

	Spheroid	Rectangular prism	Pyramid-like	Ellipsoid
0~5	12	6	20	0
5~7	31	31	35	27
7~9	34	37	25	48
≥9	21	26	20	25

(a) Length distribution of millet panicle clusters

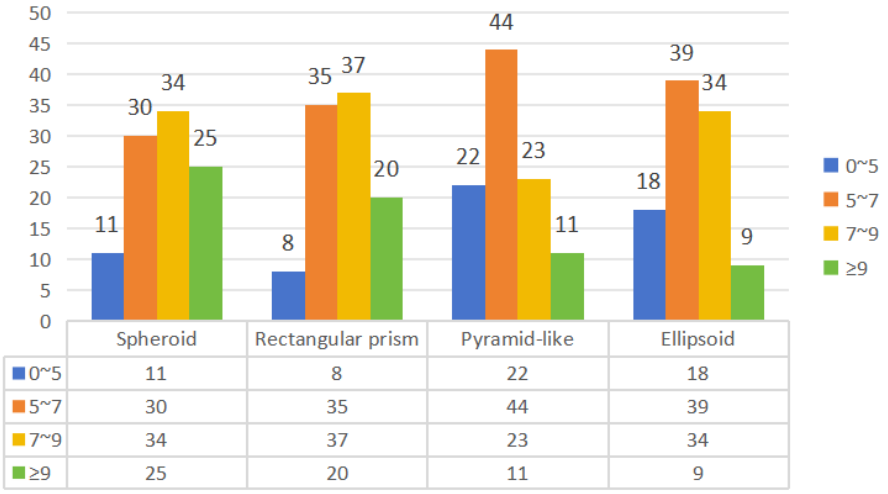

	Spheroid	Rectangular prism	Pyramid-like	Ellipsoid
0~5	11	8	22	18
5~7	30	35	44	39
7~9	34	37	23	34
≥9	25	20	11	9

(b) Width distribution of millet panicle clusters

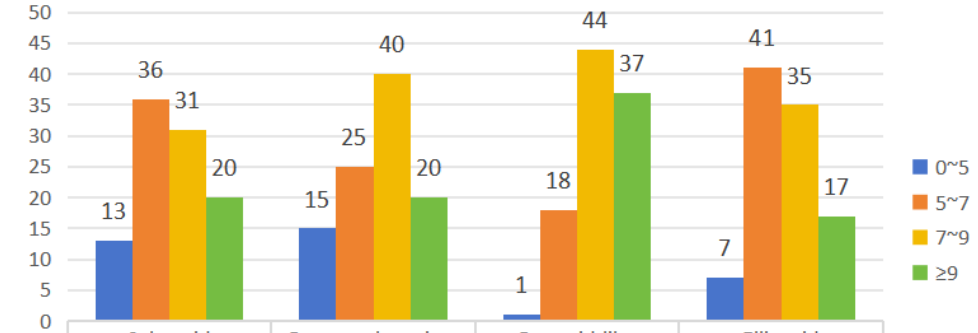

	Spheroid	Rectangular prism	Pyramid-like	Ellipsoid
0~5	13	15	1	7
5~7	36	25	18	41
7~9	31	40	44	35
≥9	20	20	37	17

(c) Height distribution of millet panicle clusters

Fig. 6 - Length, width, and height distributions of millet panicle clusters

An automatic filling method was employed for the millet panicle cluster modeling of complex-shaped and structurally variable millet panicle cluster particles. During the automatic filling process, four distinct millet panicle cluster geometric contour meshes served as boundaries, with key filling parameters set to generate equivalent particle models approximating the original data. The automatic filling settings principally comprise three parameters: the number of grid cells, the minimum particle size, and the smoothing value. In view of the complex irregularity of millet panicle cluster particle morphology and computational efficiency, this study sets the number of grid cells in all three directions to 30 and the minimum spheroid radius to 0 mm to ensure complete filling. The spheroid model employed a single-sphere filling method; however, the rectangular prism, cone, and ellipsoid models utilized automatic filling structures with smoothing values of 10, 8, and 6, respectively. The final modeling results for typical millet panicle cluster particles are illustrated in Figure 4(b).

Short Stalk Modeling

The complexity inherent in short stalk modeling can be mitigated by employing a cylindrical particle approximation with a defined length-to-diameter ratio. This approach entails the abstraction of morphological variations such as breakage or bending, thereby simplifying the modeling process. The implementation of this model involves the selection of a filling method, which can be either automatic or manual. Both of these methods have been demonstrated to effectively capture the essential structural features of short stalks. Furthermore, their application is adaptable based on the desired simulation accuracy and computational constraints, thus enhancing the model's versatility. A visual representation of the short stalk model is provided in the accompanying figure 4(b).

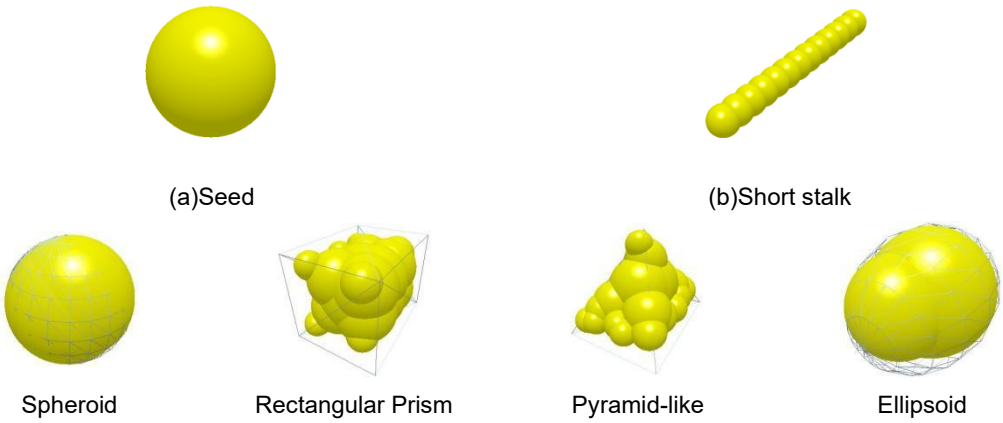

Fig. 7 - Millet Threshing Mixture Modeling Diagram

Parameter Calibration Method

Plackett–Burman design

During the process of parameter calibration, it is essential to consider the combined effects of material fundamental properties and contact mechanical characteristics on simulation accuracy in a comprehensive manner. In the present study, the fundamental parameters employed in simulation tests include Poisson's ratio, shear modulus, and density, with the specific settings detailed in Table 6. Contact parameters encompass mechanical indicators such as static friction coefficient, dynamic friction coefficient, and coefficient of restitution. In order to undertake a systematic analysis of the impact of various contact mechanical parameters on the simulated angle of repose results, to effectively reduce the number of experiments required, and to identify those factors that significantly influence the angle of repose, a Plackett–Burman experimental design was employed. With the simulated angle of repose serving as the response metric, a significance analysis of contact parameters was conducted.

Table 6

Discrete element method for simulating experimental particles and geometry base parameters

Parameters	Value	Parameters	Value
Seed Poisson's ratio	0.39	Short stalk Poisson's ratio	0.25
Seed shear modulus/（MPa）	1.46	Short stalk shear modulus/（MPa）	1.44
Seed density/（kg.m-3）	1200	Short stalk density/（kg.m-3）	300
Millet panicle cluster Poisson's ratio	0.36	45 steel plate Poisson's ratio	0.28
Millet panicle cluster shear modulus/（MPa）	0.42	45 steel plate shear modulus/（MPa）	209
Millet panicle cluster density/（kg.m-3）	800	45 steel plate density/（kg.m-3）	7850

In the calibration of seed particle parameters, six factors were identified as study variables, including the static friction coefficient between seeds, the dynamic friction coefficient between seeds, the coefficient of restitution between seeds and steel plate, and the coefficient of restitution between seeds and steel plate. Each parameter was set at two levels, with the maximum and minimum values corresponding to coding levels +1 and −1, respectively. The coding scheme is presented in Table 7.

Table 7

Plackett-Burman Test Code Table

Parameters	Low level(-1)	High level(+1)
Seed - seed static friction coefficient (A)	0.45	0.75
Seed - seed rolling friction coefficient (B)	0.01	0.09
Seed - seed coefficient of restitution (C)	0.35	0.43
Seed - 45 steel plate static friction coefficient (D)	0.40	0.70
Seed - 45 steel plate rolling friction coefficient (E)	0.01	0.05
Seed - 45 steel plate collision recovery coefficient (F)	0.35	0.50

The experimental plan was devised in accordance with the Plackett–Burman design principle. The response of the angle of repose under each set of conditions was simulated and documented, with the results shown in Table 8. By analyzing the impact of different parameter levels on the simulated angle of repose, this provides a foundation for subsequent fine calibration of key parameters.

Table 8

Plackett-Burman test program and results

Number	Factor						Angle of repose θ_1/ (°)
	A	B	C	D	E	F	
1	+1	+1	-1	+1	+1	+1	32.35
2	-1	+1	+1	-1	+1	+1	30.49
3	+1	-1	+1	+1	-1	+1	34.51
4	-1	+1	-1	+1	+1	-1	31.41
5	-1	-1	+1	-1	+1	+1	29.17
6	-1	-1	-1	+1	-1	+1	30.58
7	+1	-1	-1	-1	+1	-1	27.47
8	+1	+1	-1	-1	-1	+1	21.48
9	+1	+1	+1	+1	-1	-1	24.68
10	-1	+1	+1	-1	-1	-1	30.89
11	+1	-1	+1	+1	+1	-1	35.65
12	-1	-1	-1	-1	-1	-1	24.63

Design-Expert software was utilized to conduct significance tests and t-tests on the effects of each factor. The results of these analyses are presented in Table 9.

Table 9

Significance analysis of Plackett–Burman test results

Source	Sum of Squares	Degrees of freedom	Mean square	F-value	P-value
Model	185.89	6	30.98	18.56	0.0028
A	0.0884	1	0.0884	0.053	0.8271
B	9.56	1	9.56	5.73	0.0621
C	25.43	1	25.43	15.24	0.0114
D	117.00	1	117.00	70.10	0.0004
E	32.57	1	32.57	19.52	0.0069
F	1.24	1	1.24	0.7401	0.4289

The present study has identified the relative influence of each contact parameter on the angle of repose θ_1. Ranked from greatest to least influence, these parameters are as follows: D, E, C, B, F, A. A subsequent investigation of the P-values corresponding to each parameter reveals that the P-values associated with D and E are both less than 0.01, indicating a highly significant effect on the angle of repose. Furthermore, the P-value corresponding to C is less than 0.05, suggesting a significant influence.

Study of the Steepest Ascent Test and Parameter Optimization

According to the results of the Plackett–Burman experiment, variables A, B, and F had no significant influence on the simulated angle of repose. Therefore, their values were fixed at 0.6, 0.55, and 0.425, respectively. Further analysis indicated that factors C, D, and E were the key variables for subsequent optimization. The initial values of these factors were set at 0.01, 0.01, and 0.03, respectively, with corresponding step sizes of 0.02, 0.01, and 0.02. To identify parameter combinations closer to the measured values, a steepest ascent test was conducted. The experimental design and corresponding results are presented in Table 10.

Table 10

Experimental design and results of the steepest ascent test

Number	Parameters			Angle of repose θ_1/ (°)	Relative error δ/%
	C	D	E		
1	0.01	0.01	0.35	23.38	16.12
2	0.03	0.02	0.37	25.28	9.26
3	0.05	0.03	0.39	28.97	3.99
4	0.07	0.04	0.41	30.79	10.52
5	0.09	0.05	0.43	31.84	14.30

Based on the results of the steepest ascent test, the factor coding is presented in Table 11. The experimental design and simulation results are shown in Table 12, and the analysis of variance (ANOVA) results are presented in Table 13.

Table 11

Factor level coding for the Box–Behnken design

Factor	Low level (-1)	Middle level (0)	High level (+1)
C	0.03	0.05	0.07
D	0.02	0.03	0.04
E	0.37	0.39	0.41

Table 12

Experimental design and results of the Box–Behnken test

Number	Factor			Angle of repose θ_1/ (°)
	C	D	E	
1	-1	0	-1	26.89
2	-1	0	+1	29.69
3	+1	0	-1	29.35
4	+1	0	+1	31.49
5	0	-1	+1	26.59
6	0	-1	+1	28.77
7	0	+1	-1	30.85
8	0	+1	+1	31.75
9	-1	-1	0	25.95
10	+1	-1	0	26.74
11	-1	+1	0	27.34
12	+1	+1	0	32.38
13	0	0	0	29.46
14	0	0	0	30.11
15	0	0	0	29.61
16	0	0	0	30.26
17	0	0	0	29.89

Table 13

Analysis of variance (ANOVA) for the angle of repose of millet seeds

Source	Sum of Squares	Degrees of freedom	Mean square	F-value	P-value
Model	58.69	9	6.52	38.30	<0.0001
C	12.73	1	12.73	74.75	<0.0001
D	25.45	1	25.45	149.50	<0.0001
E	8.04	1	8.04	47.22	0.0002
CD	4.52	1	4.52	26.52	0.0013
CE	0.1089	1	0.1089	0.6396	0.4501
ED	0.4096	1	0.4096	2.41	0.1648
C2	3.79	1	3.79	22.28	0.0022
D2	2.79	1	2.79	16.40	0.0049
E2	0.8087	1	0.8087	4.75	0.0657
Residual	1.19	7	0.1703		
Lack of Fit	0.7461	3	0.2487	2.23	0.2268
Pure Error	0.4457	4	0.1114		
Total	59.88	16			

A comprehensive analysis of variance indicated that the regression model for the seed angle of repose was highly significant overall (P < 0.0001). In contrast, the lack-of-fit term was not significant (P = 0.2268), indicating that the model adequately fits the experimental data and has good predictive capability. Further analysis showed that several key parameters significantly influenced the angle of repose of seeds. These parameters included the seed–seed rolling friction coefficient (C), the seed–45 steel rolling friction coefficient (D), the seed–seed coefficient of restitution (E), the interaction term between C and D (CD), and the quadratic terms $C^2$and D^2. After eliminating non-significant factors, a regression model for predicting the seed angle of repose was established based on the significant factors. The regression equation is expressed as Eq. (8).

$$\theta_1 = 136.4014 + 301.8750\mathrm{C} + 1025.3D - 735.8375E + 5312.5000CD - 1600DE - 2373.1250C^2 - 8142.5000D^2 + 1095.625E^2 \quad (8)$$

Using the mean angle of repose of 27.34°, obtained from physical experiments, as the target value, optimal parameter back-calculation was performed based on the regression model. The optimal values of the rolling friction coefficient between seeds, the rolling friction coefficient between seeds and 45 steel, and the coefficient of restitution between seeds were determined to be 0.03, 0.04, and 0.39, respectively. Substituting these values into the model yielded a theoretical angle of repose of 27.5625°. The relative error compared with the measured value was small, indicating good agreement between the model prediction and experimental results. This result validates the accuracy and reliability of the constructed model. The EDEM simulation of pile formation and the corresponding angle of repose obtained from physical experiments are shown in Fig. 8.

Fig. 8 - EDEM simulation of seed pile formation and photograph of the seed angle of repose.

Building upon this foundation, parameter calibration simulations were conducted for millet panicle clusters, short stalks, and their mixtures, following the angle of repose calibration scheme. This enabled the sequential completion of significance analysis and optimization of key contact parameters. The final contact mechanical parameters for each component are summarized as follows. The static friction coefficient between seeds was 0.55, the dynamic friction coefficient between seeds was 0.03, and the coefficient of restitution between seeds was 0.39. The static friction coefficient between seeds and 45 steel was 0.56, the dynamic friction coefficient between seeds and 45 steel was 0.04, and the coefficient of restitution between seeds and 45 steel was 0.45. For millet panicle clusters, the static friction coefficient between clusters was 0.71, the dynamic friction coefficient was 0.05, and the coefficient of restitution was 0.28. The static friction coefficient between millet panicle clusters and 45 steel was 0.59, the dynamic friction coefficient was 0.03, and the coefficient of restitution was 0.32. For short stalks, the static friction coefficient between stalks was 0.60, the dynamic friction coefficient was 0.04, and the coefficient of restitution between stalks was 0.39. The static friction coefficient between short stalks and 45 steel was 0.61, the dynamic friction coefficient was 0.02, and the coefficient of restitution was 0.41. For mixed contacts, the static friction coefficient between seeds and millet panicle clusters was 0.52, the dynamic friction coefficient was 0.04, and the coefficient of restitution was 0.30. The static friction coefficient between seeds and short stalks was 0.58, the dynamic friction coefficient was 0.03, and the coefficient of restitution was 0.36. The static friction coefficient between millet panicle clusters and short stalks was 0.65. Simulation tests of the angle of repose were conducted using the calibrated contact parameters, yielding simulated values of 27.31°, 32.05°, and 23.86° for seeds, millet panicle clusters, and short stalks, respectively. The average deviations from the measured angles of repose were 1.94%, 3.72%, and 1.16%, respectively, demonstrating the reliability of the calibrated contact parameters.

CONCLUSIONS

This study systematically measured the geometric morphology and mechanical properties of seeds, millet panicle clusters, and short stalks from the Longgu 31 millet threshing mixture. A corresponding discrete element model was constructed, and key contact parameters were calibrated through a multi-stage experimental design. Simulation results showed that the average error between simulated and experimental values of the angle of repose was less than 5%, validating the reliability of the model and parameter system.

（1）This study overcomes the limitations of conventional single-particle modeling for grains. Based on measured statistical data, a multi-scale, proportionally scaled model with four distinct particle morphologies representing grain size within millet panicle clusters was constructed. The study also completed systematic parameter calibration for the multi-component contact system of the millet threshing mixture, filling a research gap in refined discrete element modeling of small-seeded minor grains.

（2）Parameter significance analysis demonstrated that the static friction coefficient and rolling friction coefficient between seeds and the 45 steel plate are the most critical parameters influencing the formation of the material's angle of repose. Both parameters exhibited extremely significant effects on the angle of repose, affecting material stratification, sliding, and screening behavior during the cleaning process, and thereby directly influencing simulation accuracy.

（3）The physical parameters of the millet threshing mixture and the discrete element model developed in this study provide precise data support for optimizing the screen surface structure and vibration parameters of millet cleaning equipment. This approach reduces trial-and-error costs in equipment development and establishes a solid theoretical and data foundation for improving the performance of combined harvesting and cleaning equipment for millet.

ACKNOWLEDGEMENT

This research was supported by the Heilongjiang Provincial Natural Science Foundation Young Scientist Program (QC2025E046), the Heilongjiang Provincial Postdoctoral Science Foundation (LBH-Z24251), the Guiding Science and Technology Project of Daqing City (zd-2025-033), the Research Start-up Program for Returned and Introduced Talents (XYB202309), and the "Sanzong" Youth Innovation Talent Program (ZRCQC202304).

REFERENCES

[1] Ao R., Zhang W., Wang S., Liu W., & Yu Z. (2023). Measurement of Physical Contact Parameters and Discrete Element Simulation Calibration of Sunflower Seeds. *Journal of Agricultural Mechanization Research*, Vol.45, Issue 4, pp.139-147.

[2] Awuah E., Aikins K.A., Antille D.L., Zhou J., Gbenontin B.V., Mecha P., &Liang Z. (2023). Discrete Element Method Simulation and Field Evaluation of a Vibrating Root-Tuber Shovel in Cohesive and Frictional Soils. *Agriculture*, Vol.13, Issue 8, pp.1525.

[3] Chang Z., Wang Y., Feng L., Zhang L., Guo P., & Yuan X. (2020). Effects of sowing parameters of millet precision seeder on growth characteristics and yield of Jingu 21. *Transactions of the Chinese Society of Agricultural Engineering*, Vol.36, Issue 12, pp.22-29.

[4] Chen L., Shen K., Li J., Wan H., Cao C., Hu S., & Li Z. (2025). Parameter Calibration and Experiment Verification of Shrimp Feed Pellet Based on Discrete Element Method. *Transactions of the Chinese Society for Agricultural Machinery*, Vol. 56, Issue 12, pp. 750-760.

[5] Gao B., Zhai Z., Lan Y., Pei G., Zhao L. (2024). Power Consumption Prediction Model of Forage Crusher Based on DEM-BPM-CFD Coupling Method. *Transactions of the Chinese Society for Agricultural Machinery*, Vol. 55, Issue S2, pp. 168-176.

[6] Li H., Guo G., Xun L., Lu J., Chen H., &Cui G. (2025). The Establishment of a Discrete Element Model of Wheat Grains with Different Moisture Contents: A Research Study. *Agriculture*, Vol.15, Issue 11, pp.1232.

[7] Li H., Meng Y., Qi X., Wang Y., Li Q. & Li M. (2025). Discrete Element Modelling Method and Parameter Calibration of Garlic Species Based on Bonding V2 Model. *Transactions of the Chinese Society for Agricultural Machinery*, Vol.56, Issue 7, pp.150-157+169.

[8] Li X., Wang W., Zhao G., Sun C., Hu Z., & Ji J. (2021). Design and Experiment of Longitudinal Axial Flow Double Flexible Rolling and Kneading Threshing Device for Millet. *Transactions of the Chinese Society for Agricultural Machinery*, Vol. 52, Issue 7, pp. 113-123.

[9] Li Y., Chen Y., Sun X., Lin H., & He J. (2025). Parameter calibration of the breakable flexible fiber model for maize stovers with different moisture contents. *Transactions of the Chinese Society of Agricultural Engineering*, Vol.41, Issue 3, pp.43-52.

[10] Liu Y., Yi S., Li Y., Tao G., Mao X. &Zhang D. (2023). Design and Performance Test of Millet Threshing and Separation Equipment. Journal of Agricultural Mechanization Research, Vol.45, Issue 9, pp.165-170.

[11] Liu Z., Zhang L., Peng F. (2025). Calibration and experiment of the contact parameters of walnut kernels based on discrete element simulation. *Transactions of the Chinese Society of Agricultural Engineering*, Vol.41, Issue 22, pp.316-324.

[12] Shen W., Xia R., Huang J., & Wang Y. (2026). Research on simulation method and experimental verification of composite L-joints. *Journal of Huazhong University of Science and Technology (Natural Science Edition)*, Vol.54, Issue 1, pp.156-160.

[13] Shi T., Zhang C., Li Z., & Cui L. (2026). Parameter Calibration of Discrete Element Model of Polygonum Cuspidatum Rhizome. *Journal of Agricultural Mechanization Research*, Vol.48, Issue 4, pp.118-125+135.

[14] Shu C., Yang J., Wan X., Yuan J., Liao Y. & Liao Q. (2022). Calibration and experiment of the discrete element simulation parameters of rape threshing mixture in combine harvester. *Transactions of the Chinese Society of Agricultural Engineering*, Vol.38, Issue 9, pp.34-43.

[15] Sun J., Yang Z., Guo Y., Cui Q., Wu X., & Zhang Y. (2017). Compression mechanical properties and crack formation law of millet grain. *Transactions of the Chinese Society of Agricultural Engineering*, Vol. 33, Issue 18, pp. 306-314.
[16] Sun K., He C., Zhou Q., Yu X., Dong Q., Wang W., Chen Y., Li M., Xia X., Wang Y., & Zhou L. (2024). Study on the Influence Mechanism of Soil Covering and Compaction Process on Maize Sowing Uniformity Based on DEM–MBD Coupling. *Agronomy*, Vol.14, Issue 12, pp.2883.
[17] Tao X. (2025). Design and Testing of a Grain Seed Cleaning Device. *Journal of Agricultural Mechanization Research*, Vol.47, Issue 3, pp.152-157.
[18] Wang X., Lin W., Liu G., Ma S., & Tong R. (2020). Advance in Impact Force Model Research with Evolution of Newton Restitution Coefficient. *Mechanical Science and Technology for Aerospace Engineering*, Vol.39, Issue 10, pp.1526-1533.
[19] Wensrich C., & Katterfeld A. (2012). Rolling friction as a technique for modelling particle shape in DEM. *Powder Technology*, Vol.217, pp.409-417.
[20] Xie B., Bai J., Yan J., Zhao S., Liu N., & Zhang Q. (2023). Calibration of white rice simulation parameters based on discrete element method. *INMATEH-Agricultural Engineering*, Vol.71, Issue 3, pp.215-224.
[21] Xu B., Zhang Y., Cui Q., Ye S., & Zhao F. (2021). Construction of a discrete element model of buckwheat seeds and calibration of parameters. *INMATEH-Agricultural Engineering*, Vol.64, Issue 2, pp.175-184.
[22] Xu Y., Lv M., Gui J., Li J., & Zhang D. (2023). Applicability of BRUTSAERT's model in soil moisture detection. *Transactions of the Chinese Society of Agricultural Engineering*, Vol.39, Issue 21, pp.54-65.
[23] Xun X., Feng M., Wu C., Jia J., &Chen J. (2025). Construction and Experiment of Discrete Element Model for Tea Garden Soil-Organic Fertilizer Mixture Based on EDEM. *Transactions of the Chinese Society for Agricultural Machinery*, Vol.56, Issue 12, pp.267-278.
[24] Yang Z., Guo Y., Cui Q., & Li H. (2016). Test and influence factors analysis of friction characteristics of millet. *Transactions of the Chinese Society of Agricultural Engineering*, Vol.32, Issue 16, pp.258-264.